PERGAMON

International Journal of Heat and Mass Transfer 45 (2002) 923–929

International Journal of HEAT and MASS TRANSFER

www.elsevier.com/locate/ijhmt

Technical Note

Thermal entry region analysis through the finite integral transform technique in laminar flow of Bingham fluids within concentric annular ducts

U.C.S. Nascimento [a], E.N. Macêdo [b], J.N.N. Quaresma [a,*]

[a] *Chemical Engineering Department – CT, Universidade Federal do Pará – UFPA, Campus Universitário do Guamá, Rua Augusto Corrêa, 01, 66075-900 Belém, PA, Brazil*

[b] *Mechanical Engineering Department – CT, Universidade Federal do Pará – UFPA, Campus Universitário do Guamá, Rua Augusto Corrêa, 01, 66075-900 Belém, PA, Brazil*

Received 7 July 2000; received in revised form 29 May 2001

Abstract

The heat transfer characteristics of Bingham plastics fluids within concentric annular ducts are analytically studied through the classical finite integral transform technique. In the analysis of the thermal entry region, four types of boundary conditions are adopted and prescribed either at the inner or outer duct wall, and the flow is considered to be laminar and fully developed. Local Nusselt numbers are computed along the channel length with high accuracy for different values of aspect ratios and yield numbers, which are systematically tabulated and graphically presented. Comparisons with previous works in the literature are also performed for typical situations, in order to validate the numerical codes developed in this work, as well as to demonstrate that consistent results were produced.

1. Introduction

The analysis of the heat and fluid flow characteristics involving viscoplastic materials within annular ducts plays an important role in the design of thermal-hydraulic equipment, since there are numerous industrial applications related to these fluids. Fluids included into this category are those that follow the Herschel–Bulkley model or a Bingham plastic model, which present in their constitutive equations a yield stress, which must be exceeded in order to start the flow [1,2].

A literature survey reveals that such analyses are mostly concerned to the flow of viscoplastic materials in circular tubes and parallel-plates channels [3–10]. Therefore, in this context, in order to fill out the gap presented in the literature for the heat transfer convection of Bingham plastic fluids within concentric annular ducts, the present work aims at advancing the ideas in the classical and generalized integral transform techniques and the so-called sign-count method to determine Nusselt numbers along both, the thermal entry and fully developed regions, with high accuracy. Four kinds of boundary conditions are adopted for this thermal problem, furnishing a broad analysis of the problem. Numerical results are obtained for different values of aspect ratios and yield numbers, showing the importance of the duct geometric configuration and the fluid rheology on the Nusselt numbers.

2. Analysis

In order to analyze the heat transfer problem of a non-Newtonian fluid that follows the Bingham plastic model, one considers steady forced convection in thermally developing, hydrodynamically developed laminar flow within a concentric annular duct (details in

* Corresponding author.
E-mail address: quaresma@ufpa.br (J.N.N. Quaresma).

0017-9310/02/$ - see front matter
PII: S0017-9310(01)00187-9

Nomenclature

D_h	hydraulic diameter; $= 2(r_{ow} - r_{iw})$
$Nu_{iw}(Z), Nu_{ow}(Z)$	local Nusselt numbers at inner and outer walls, respectively
q''_{iw}, q''_{ow}	prescribed heat fluxes at inner and outer walls, respectively
r, R	radial coordinates, dimensional and dimensionless, respectively
r_{iw}, r_{ow}	inner and outer radii, respectively
$T(r,z)$	temperature distribution, dimensional
T_{iw}, T_{ow}	prescribed temperatures at inner and outer walls, respectively
u_{av}	average flow velocity
$u(r), U(R)$	velocity distributions, dimensional and dimensionless, respectively
Y	yield number; $= \tau_0 D_h/\mu_0 u_{av}$
z, Z	axial coordinates, dimensional and dimensionless, respectively
Greek symbols	
$\theta(R,Z)$	dimensionless temperature distribution
$\theta_{av}(Z)$	dimensionless average temperatures
$\theta_{iw}(Z)$, $\theta_{ow}(Z)$	dimensionless temperature at inner and outer walls, respectively
μ_0	plastic viscosity of the fluid
τ_0	yield stress

obtaining the velocity field can be found in [11]). Viscous dissipation, free convection, and axial conduction effects are neglected, and physical properties are taken as constant. The duct walls are subjected to different boundary conditions (see [12] for more details), and the fluid enters the channel with a uniform temperature, T_e. Then, the mathematical formulation for this convective heat transfer problem in dimensionless form is written as:

$$W(R)\frac{\partial\theta(R,Z)}{\partial Z} = \frac{\partial}{\partial R}\left[R\frac{\partial\theta(R,Z)}{\partial R}\right] \quad \text{in } \gamma < R < 1,\ Z > 0, \tag{1a}$$

$$\theta(R,0) = 0, \quad \gamma \leqslant R \leqslant 1, \tag{1b}$$

$$\theta(\gamma,Z) = 1 - m, \quad Z > 0, \tag{1c}$$

$$\theta(1,Z) = m, \quad Z > 0, \tag{1d}$$

where in the boundary conditions (1c) and (1d), the coefficient m identifies whether it refers to case A ($m = 1$) or to case B ($m = 0$). In addition, the following dimensionless groups were used:

$$R = \frac{r}{r_{ow}}; \quad \gamma = \frac{r_{iw}}{r_{ow}}; \quad U(R) = \frac{u(r)}{u_{av}}, \tag{2a–c}$$

$$W(R) = \frac{RU(R)}{4(1-\gamma)^2}; \qquad Z = \frac{z}{D_h Re Pr}, \tag{2d, e}$$

$$Re = \frac{u_{av} D_h \rho}{\mu_0}; \qquad Pr = \frac{\mu_0 c_p}{k}, \tag{2f, g}$$

$$\theta(R,Z) = \frac{T(r,z) - T_e}{T_{ow} - T_e} \quad \text{with } T_{iw} = T_e,\ m = 1 \tag{2h}$$

or

$$\theta(R,Z) = \frac{T(r,z) - T_e}{T_{iw} - T_e} \quad \text{with } T_{ow} = T_e,\ m = 0. \tag{2i}$$

The solution of the heat transfer problem given by Eqs. (1a)–(1d) is obtained through the classical integral transform technique [13,14]. Then, the complete solution for the potential $\theta(R,Z)$ is obtained by the approach cited above, for boundary conditions of first kind, in the form [11]:

$$\theta(R,Z) = \theta_p(R) + \sum_{i=1}^{\infty} \frac{\bar{f}_i}{N_i}\psi_i(R)\exp(-\mu_i^2 Z);$$

$$\theta_p(R) = m + (1-2m)\frac{\ln R}{\ln \gamma}, \tag{3a, b}$$

$$\bar{f}_i = -\int_{\gamma}^{1} W(R)\psi_i(R)\theta_p(R)\,dR;$$

$$N_i = \int_{\gamma}^{1} W(R)\psi_i^2(R)\,dR, \tag{3c, d}$$

where $\psi_i(R)$ and μ_i are the eigenfunctions and eigenvalues, respectively, of an appropriate eigenvalue problem. Fundamental solutions for other types of boundary conditions are obtained following the same procedure as applied for boundary conditions of first kind, and are written as:

$$\theta(R,Z) = \theta_{av}(Z) + \theta_p(R) + \sum_{i=1}^{\infty} \frac{\bar{f}_i}{N_i}\psi_i(R)\exp(-\mu_i^2 Z), \tag{4a}$$

$$\theta_{av}(Z) = \frac{4Z[m + \gamma(1-m)]}{(1+\gamma)}, \tag{4b}$$

$$\theta_p(R) = \frac{32[m+\gamma(1-m)](1-\gamma)}{(1+\gamma)^2} \times \int_\gamma^1 W(R)\left\{\int_R^1 \frac{1}{\zeta}\left[\int_\gamma^\zeta W(\eta)\,d\eta\right]d\zeta\right\}dR + \frac{4\gamma(1-m)}{(1+\gamma)}\left(\int_\gamma^1 W(R)\ln R\,dR\right) - \frac{4[m+\gamma(1-m)]}{(1+\gamma)}\int_R^1 \frac{1}{\zeta}\left[\int_\gamma^\zeta W(\eta)\,d\eta\right]d\zeta - \frac{\gamma(1-m)}{2(1-\gamma)}\ln R \quad \text{(second kind)}, \tag{4c}$$

$$\theta(R,Z) = \theta_p(R) + \sum_{i=1}^{\infty}\frac{\bar{f}_i}{N_i}\psi_i(R)\exp(-\mu_i^2 Z), \tag{5a}$$

$$\theta_p(R) = 1 \quad \text{(third kind)}, \tag{5b}$$

$$\theta(R,Z) = \theta_p(R) + \sum_{i=1}^{\infty}\frac{\bar{f}_i}{N_i}\psi_i(R)\exp(-\mu_i^2 Z), \tag{6a}$$

$$\theta_p(R) = \frac{m\ln(R/\gamma)}{2(1-\gamma)} - \frac{(1-m)\gamma\ln R}{2(1-\gamma)} \quad \text{(fourth kind)}. \tag{6b}$$

At this point, quantities of practical interest, such as average temperature and local Nusselt numbers at the inner and outer channel walls can be determined from Eqs. (4a)–(6b) according to their definitions given in [12]. For the case of boundary conditions of second kind, the average temperature is determined a priori, and is given by Eq. (4b).

3. Results and discussion

Computational codes were developed in the FORTRAN programming language and implemented on a PENTIUM II 400 MHz computer platform. Numerical results were produced for Nusselt numbers with different yield numbers and aspect ratios, and by adopting the four different types of boundary conditions.

In order to validate the numerical code developed in the present work, and to demonstrate its numerical consistency, Table 1 shows a comparison of the present results for Newtonian fluids, by adopting the four types of boundary conditions, against those presented by Shah and London [12], in the thermal entry region for the aspect ratio $\gamma = 0.1$. From this table, it can be observed that the results are in excellent agreement, furnishing a plain direct validation of the computational code developed in the present work.

3.1. Effect of yield number

Figs. 1–4 present results for local Nusselt numbers distributions along both the thermal entry and fully developed regions, for different values of yield numbers ($Y = 0$, 1, 5 and 10), and aspect ratios ($\gamma = 0.1$ and 0.9), corresponding to the four pairs of boundary conditions adopted. It is verified that in the thermal entry region, an increase in the Y parameter results on higher values for the local Nusselt number, for all cases of thermal boundary conditions analyzed. This effect in the fully developed region practically disappears, where in graphic scale, the values of Nusselt numbers are coincident. The influence on the thermal entry region can mainly be explained through the velocity field presented in [11], there it can be observed that for increasing Y values, the plug-flow region increases, as a result the velocity gradients near the walls tend to become more pronounced, and consequently, the heat exchange is intensified in such regions, resulting in greater values for Nusselt numbers. The magnitude of the local Nusselt number either at the inner or at the outer wall depends on the position of these velocity gradients, for instance, for boundary conditions of first kind, considering the aspect ratio $\gamma = 0.1$, in the fully developed region the local Nusselt number presents greater values at the inner wall than at the outer one, since the velocity gradients are greater at that wall.

3.2. Effect of channel geometry

Concentric annular duct has two limit configuration cases, i.e., when the aspect ratio, $\gamma \to 0$, the duct tends to be represented by a circular tube, and when $\gamma \to 1$, by a parallel-plates channel. In both situations, the velocity and temperature distributions become symmetrical. The aspect ratio effect is evident when Figs. 1 and 4 are analyzed. It can be observed that as the aspect ratio increases, the local Nusselt numbers at the inner and outer walls tend to the same values, since at higher values of aspect ratios, for example, $\gamma = 0.9$, the velocity and temperature profiles show a certain symmetry, because of the geometric configuration of the channel.

3.3. Effect of thermal boundary conditions

In all cases of thermal boundary conditions analyzed, the local Nusselt numbers at the inner and outer walls either increase or decrease along the thermal entry region tending to an asymptotic value corresponding to that of the fully developed region.

In the case of boundary conditions of the first kind, the local Nusselt numbers at the outer wall decrease and reach an asymptotic value, whereas at the inner wall the local Nusselt numbers increase and reach asymptotic values greater than those at the outer wall. This can be explained by the fact that the velocity profile is steeper near to the inner wall than the outer one [11], leading to greater heat transfer rates at this region. This effect diminishes as the

Table 1
Thermal parameters computed from the present analysis for the four types of boundary conditions adopted (Newtonian case and $\gamma = 0.1$)

Z	Case 1A			Case 1B		
	$Nu_{iw}(Z)$	$Nu_{ow}(Z)$	$\theta_{av}(Z)$	$Nu_{iw}(Z)$	$Nu_{ow}(Z)$	$\theta_{av}(Z)$
1.0E−5		52.340[a]	0.00282[a]	80.328[a]		0.00047[a]
	–[c]	52.336[b]	0.00287[b]	80.324[b]	–[c]	0.00043[b]
1.0E−3		10.913	0.05827	22.257		0.01099
	–[c]	10.912	0.05832	22.192	–[c]	0.01094
1.0E−2	0.1661[a]	5.3590	0.24529	13.761	0.0664[a]	0.06134
	0.1550[b]	5.3590	0.24530	13.762	0.0664[b]	0.06131
∞	10.459	3.0953	0.74744	10.459	3.0953	0.25256
	10.459	3.0950	0.74744	10.459	3.0950	0.25256
Z	Case 2A			Case 2B		
	$Nu_{ow}(Z)$	$\theta_{iw}(Z)$	$\theta_{ow}(Z)$	$Nu_{iw}(Z)$	θ_{iw} (Z)	$\theta_{ow}(Z)$
5.0E−5	36.939[a]		0.027253[a]	58.020[a]	0.017254[a]	
	36.940[b]	–[c]	0.027252[b]	58.019[b]	0.017254[b]	–[c]
5.0E−3	8.0832		0.141895	17.117	0.060238	
	8.0830	–[c]	0.141892	17.120	0.06024	–[c]
5.0E−2	4.9610	0.074622[a]	0.383391	12.128	0.100634	0.007462[a]
	4.9610	0.074621[b]	0.383391	12.128	0.100634	0.007642[b]
∞	4.8342	∞	∞	11.906	∞	∞
	4.8340			11.906		
Z	Case 3A			Case 3B		
	$Nu_{ow}(Z)$	$\theta_{iw}(Z)$	$\theta_{av}(Z)$	$Nu_{iw}(Z)$	$\theta_{ow}(Z)$	$\theta_{av}(Z)$
1.0E−2	5.3589[a]	0.00149[a]	0.24525[a]	13.761[a]	0.00071[a]	0.06209[a]
	5.3590[b]	0.00153[b]	0.24535[b]	13.762[b]	0.00032[b]	0.06122[b]
1.0E−1	4.1140	0.68398	0.81289	11.561	0.26945	0.36352
	4.1140	0.68400	0.81292	11.562	0.26918	0.36295
5.0E−1	4.1135	0.99920	0.99953	11.559	0.86401	0.88153
	4.1140	0.99920	0.99953	11.560	0.86398	0.88144
∞	4.1135	1	1	11.559	1	1
	4.1140	1	1	11.560	1	1
Z	Case 4A			Case 4B		
	$Nu_{iw}(Z)$	$Nu_{ow}(Z)$	$\theta_{av}(Z)$	$Nu_{iw}(Z)$	$Nu_{ow}(Z)$	$\theta_{av}(Z)$
1.0E−2	0.1932[a]	6.6681[a]	0.036732[a]	14.902[a]	0.0409[a]	0.003634[a]
	0.0340[b]	6.6460[b]	0.036254[b]	14.902[b]	0.0420[b]	0.003636[b]
1.0E − 1	8.3142	4.3559	0.324084	11.072	2.7777	0.024624
	8.3090	4.3500	0.323770	11.072	2.7780	0.024625
5.0E−1	10.304	3.2714	0.838497	10.460	3.0947	0.032288
	10.304	3.2710	0.838450	10.460	3.0950	0.032288
∞	10.459	3.0953	0.956141	10.459	3.0953	0.032307
	10.459	3.0950	0.956140	10.459	3.0950	0.032307

[a] Present work.
[b] [12].
[c] Not available.

aspect ratio increases, since the velocity profiles tend towards becoming symmetric thus resulting in a near-symmetry for the local Nusselt numbers in the thermally fully developed region. It is important to note that for case 1A, the local Nusselt number at the inner wall is practically null in regions near the channel entry, since for this case the inner wall temperature is equal to the fluid inlet temperature, resulting in heat exchanges occurring only in positions far away from the channel entry. The same verification is observed for the case 1B, however, for the Nusselt number at the outer wall.

This same analysis is also verified for the case of boundary conditions of fourth kind. A comparison of Nusselt numbers at the inner and outer walls for cases 1A and 1B, in the thermal entry region, shows that case 1B presents greater Nusselt numbers at the inner wall. The explanation for this fact is that the inner wall has a

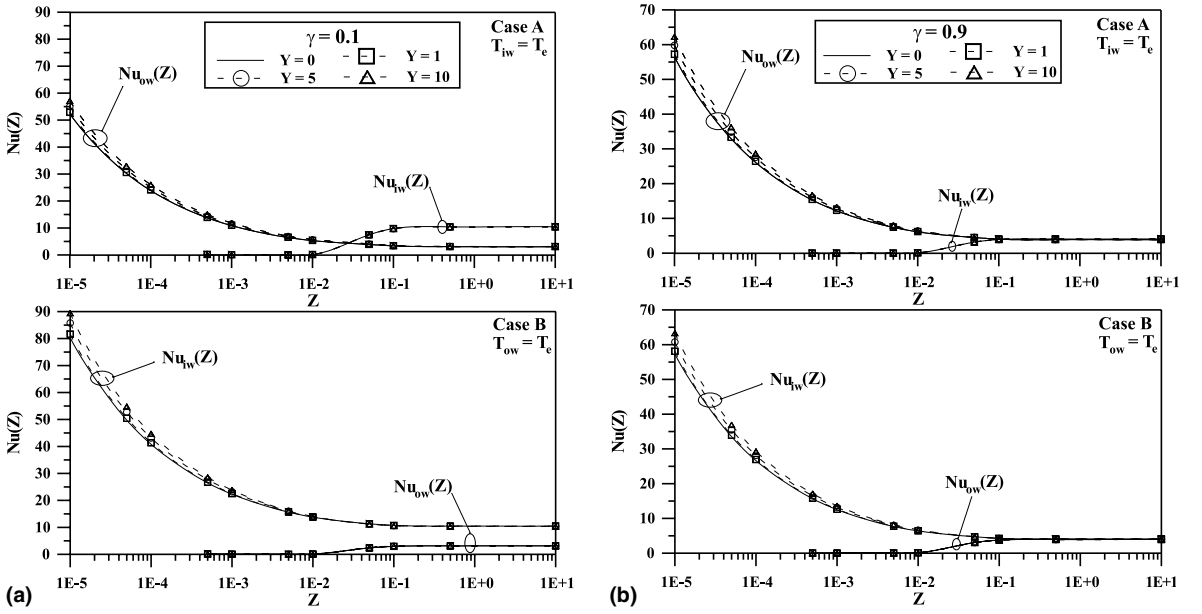

Fig. 1. Local Nusselt numbers in the thermal entry region for different values of yield numbers for the case of boundary conditions of first kind: (a) $\gamma = 0.1$; (b) $\gamma = 0.9$.

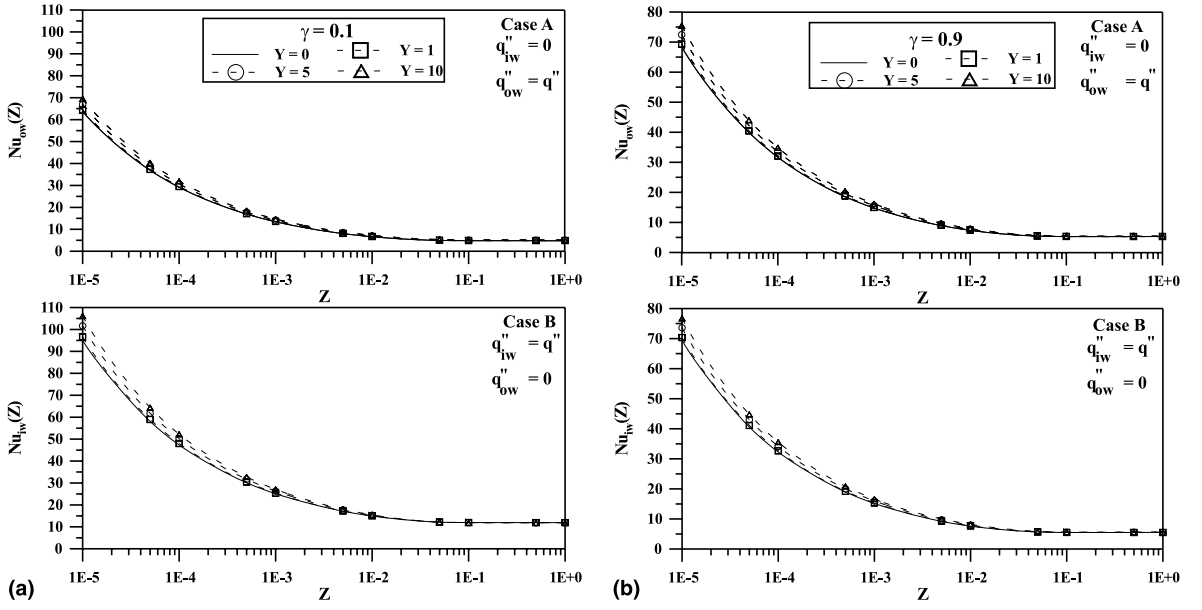

Fig. 2. Local Nusselt numbers in the thermal entry region for different values of yield numbers for the case of boundary conditions of second kind: (a) $\gamma = 0.1$; (b) $\gamma = 0.9$.

smaller area, and thus, greater heat fluxes are obtained compared with the outer wall, and consequently, as the Nusselt numbers are directly proportional to the heat flux, greater values are also obtained for this thermal parameter.

The case of boundary conditions of second kind presents a similar analysis as the third kind one. Both of them have null local Nusselt numbers when there is no heat flux. Once more, the symmetry in Nusselt numbers profiles is verified for higher values of the aspect ratio,

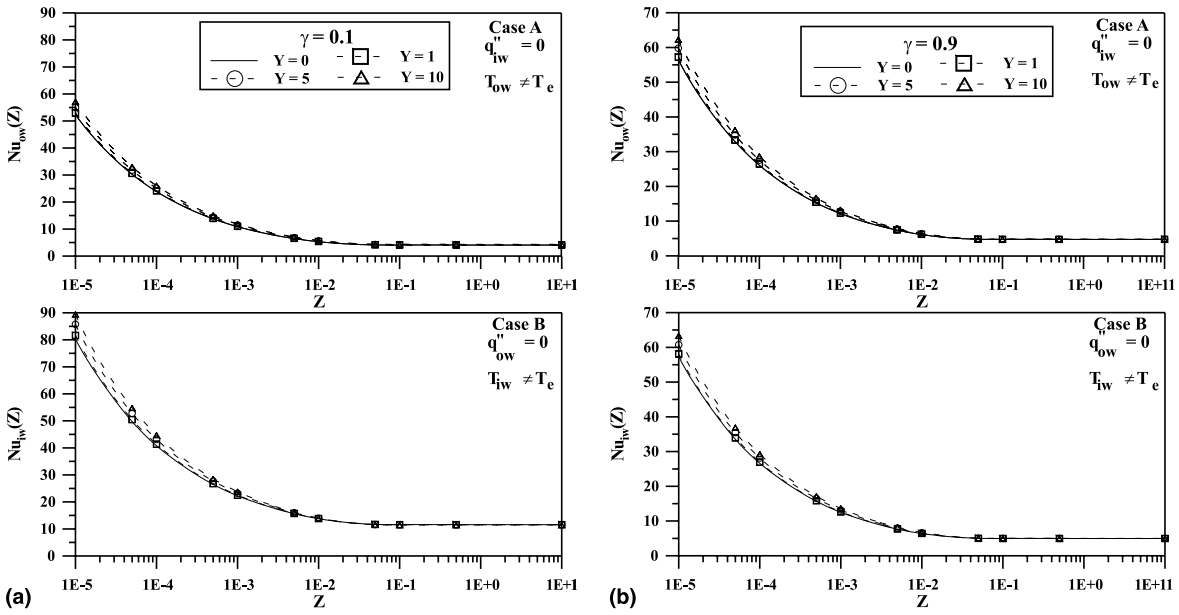

Fig. 3. Local Nusselt numbers in the thermal entry region for different values of yield numbers for the case of boundary conditions of third kind: (a) $\gamma = 0.1$; (b) $\gamma = 0.9$.

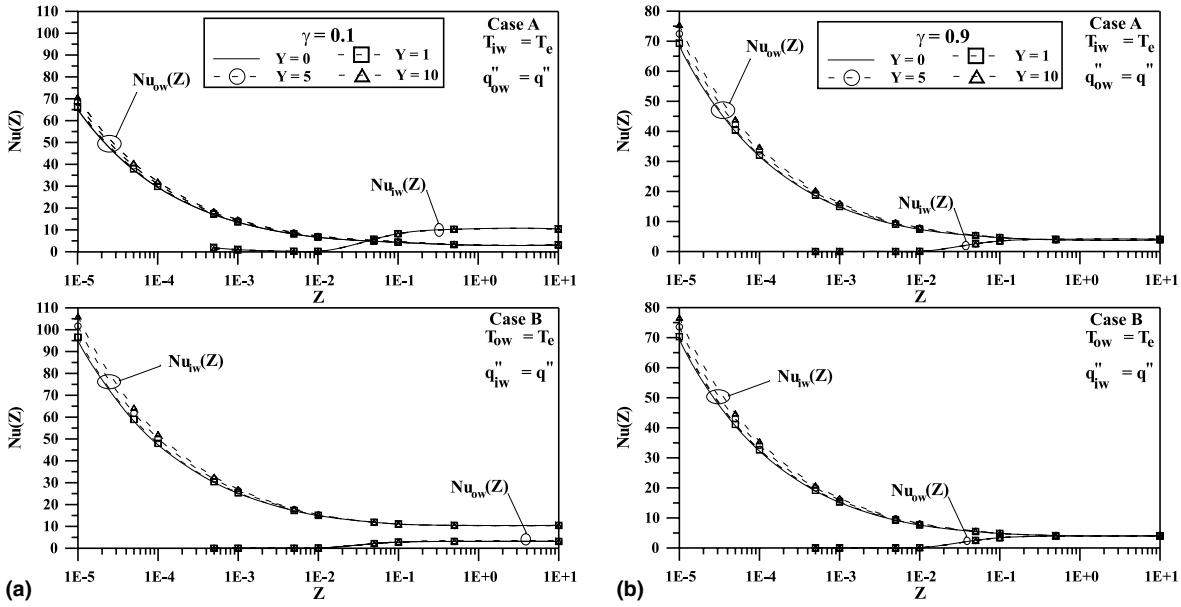

Fig. 4. Local Nusselt numbers in the thermal entry region for different values of yield numbers for the case of boundary conditions of fourth kind: (a) $\gamma = 0.1$; (b) $\gamma = 0.9$.

such as that presented in Fig. 2(b) for an aspect ratio $\gamma = 0.9$, where the Nusselt numbers distributions at the inner and outer walls corresponding to the cases 2B and 2A, respectively, present the same distribution along the channel length. This fact can also be verified in Fig. 3(b) for the cases 3A and 3B. For boundary conditions of the fourth kind, the local Nusselt numbers distributions present a behavior similar to those of boundary conditions of first kind.

Finally, it is also important to notice that for the cases where constant heat fluxes at the walls (cases 2 and 4) were adopted as boundary conditions, greater values

for the local Nusselt numbers were obtained compared to the cases of prescribed wall temperatures (cases 1 and 3), as can be observed by comparing Figs. 1 and 4, or by comparing Figs. 2 and 3, respectively.

References

[1] R.B. Bird, R.C. Armstrong, O. Hassager, Dynamics of Polymeric Liquids, second ed., vol. 1, Wiley, New York, 1987.
[2] R.B. Bird, G.C. Dai, B.J. Yarusso, The rheology and flow of viscoplastic materials, Rev. Chem. Eng. 1 (1983) 1–70.
[3] W.J. Laird, Slurry and suspension transport, Ind. Eng. Chem. 49 (1957) 138–141.
[4] A.G. Fredrickson, R.B. Bird, Non-Newtonian flow in annuli, Ind. Eng. Chem. 50 (1958) 347–383.
[5] B.E. Anshus, Bingham plastic flow in annuli, Ind. Eng. Chem. Fundam. 13 (1974) 162–164.
[6] G. Forrest, W.L. Wilkinson, Laminar heat transfer to temperature-dependent Bingham fluids in tubes, Int. J. Heat Mass Transfer 16 (1973) 2377–2391.
[7] B.F. Blackwell, Numerical solution of the Graetz problem for a Bingham plastic in laminar tube flow with constant wall temperature, J. Heat Transfer 107 (1985) 466–468.
[8] G.C. Vradis, J. Dougher, S. Kumar, Entrance pipe flow and heat transfer for a Bingham plastic, Int. J. Heat Mass Transfer 36 (1993) 543–552.
[9] C. Nouar, R. Devienne, M. Lebouché, Convection thermique pour un fluide de Herschel–Bulkley dans la région d'entrée d'une conduite, Int. J. Heat Mass Transfer 37 (1994) 1–12.
[10] M. Soares, M.F. Naccache, P.R.S. Mendes, Heat transfer to viscoplastic materials flowing laminarly in the entrance region of tubes, Int. J. Heat Fluid Flow 20 (1999) 60–67.
[11] U.C.S. Nascimento, E.N. Macêdo, J.N.N. Quaresma, Solution for the thermal entry region in laminar flow of Bingham plastics within annular ducts via integral transformation, Hybrid Meth. Eng. 2 (2000) 233–247.
[12] R.K. Shah, A.L. London, Laminar flow forced convection in ducts, Adv. Heat Transfer (suppl. 1) (1978).
[13] M.D. Mikhailov, M.N. Özisik, Unified Analysis and Solutions of Heat and Mass Diffusion, Wiley, New York, 1984.
[14] R.M. Cotta, Integral Transforms in Computational Heat and Fluid Flow, CRC Press, Boca Raton, 1993.